Appl Phys A (2009) 97: 19–23
DOI 10.1007/s00339-009-5352-6

Applied Physics A
Materials Science & Processing

RAPID COMMUNICATION

Characterization of thermal transport in micro/nanoscale wires by steady-state electro-Raman-thermal technique

Yanan Yue · Gyula Eres · Xinwei Wang · Liying Guo

Received: 13 July 2009 / Accepted: 16 July 2009 / Published online: 28 July 2009

Abstract In this work, a novel steady-state electro-Raman-thermal (SERT) technique is developed to characterize the thermal transport in one-dimensional micro/nanoscale materials. The SERT technique involves steady-state joule heating of a suspended sample and measuring its middle point temperature based on the temperature dependence of the Raman shift peak intensity. The thermal conductivity is determined from a linear fitting of the temperature against heating power. Multi-wall carbon nanotube bundles are characterized using the SERT technique to verify its measurement capacity. As it does not need to track the transient process of heat transfer, the SERT technique has the great potential for measuring short materials down to nm long.

PACS 65.80.+n · 66.30.Xj · 06.30.Dr · 43.20.Ye

1 Introduction

As one-dimensional nanoscale material, carbon nanotubes (CNTs) are attracting high attention because of their unique structures and excellent mechanical, electrical, optical and thermal characteristics. Several non-contact techniques, such as the 3ω method, the microfabricated device method, the optical heating electrical thermal sensing (OHETS) technique, the transient electrothermal (TET) technique, the transient photo-electrothermal (TPET) technique and the pulsed laser-assisted thermal relaxation (PLTR) technique have been developed on measuring the thermophysical properties of different kinds of CNTs and micro/nanowires [1–8]. In these techniques, the 3ω method uses the specimen as both heater and thermometer to study its resistance change with temperature by analyzing the 3ω signal [1]. The OHETS method employs a modulated laser to heat the sample and detects the resistance change by monitoring the voltage variation [4]. The TET, TPET and PLTR techniques probe the temperature evolution during step electrical/laser heating or after pulsed laser heating to evaluate the thermal diffusivity [5–8].

Our past work has demonstrated that the OHETS, TET, TPET and PLTR techniques feature superior measurement accuracy and significantly reduced experiment time over the 3ω technique. Usually a long time is required in the OHETS experiment [4]. In the transient techniques such as TET, TPET, and PLTR, the thermal relaxation time of the sample is $\sim l^2/\alpha$, where l is the sample length and α is its thermal diffusivity. For samples of very short length and high thermal diffusivity, the characteristic heat transfer time could become very short and it becomes difficult to employ the transient techniques. In addition, these techniques have no capacity for direct temperature measurement, while such a measurement is very critical for analyzing the heat transfer process in the material and determining its thermal conductivity. To overcome the challenges mentioned above, in this work we develop a new advanced technique: steady-state electro-Raman-thermal (SERT) technique, which directly measures the temperature of micro/nanowires under steady-state joule heating. The combined steady-state electric heating and temperature measurement based on the Ra-

Y. Yue · X. Wang (✉) · L. Guo
Department of Mechanical Engineering, Iowa State University, 2025 Black Engineering Building, Ames, IA 50011-2161, USA
e-mail: xwang3@iastate.edu
Fax: +1-515-2943261

G. Eres
Materials Science and Technology Division, Oak Ridge National Laboratory, 1 Bethel Valley Road, MS-6056, Oak Ridge, TN 37831-6056, USA

man signal lead to direct characterization of the thermal conductivity of the sample. In this paper, two multi-wall CNT (MWCNT) bundles are measured to demonstrate the strong capability of the SERT technique.

2 Experimental principle and details

In this SERT technique, the conductive micro/nanowire of length $2L$ is suspended between two electrodes. A DC current I is passed through the sample to induce steady-state electrical heating. Because the electrodes are excellent heat sinks due to their large size in comparison with the sample, the connection points between wires and electrodes will stay at room temperature (T_0). Under the circumstance that the wire is placed in a vacuum, only heat conduction along the wire is important, and the thermal radiation from the wire is negligible. Therefore, the temperature distribution along the wire can be described as $T(x) = I^2 \cdot R \cdot L/(4k \cdot A_c) \cdot (1 - x^2/L^2) + T_0$, where R, k, A_c are the electrical resistance, thermal conductivity, and the cross-sectional area of the wire, respectively. x is the coordinate along the wire with its origin in its middle point. At this point of the wire, the temperature is $T(0) = I^2 \cdot R \cdot L/(4k \cdot A_c) + T_0$. Theoretically, by only measuring this middle point temperature, the thermal conductivity of the sample can be determined directly. To suppress the uncertainty in the temperature measurement, different electrical currents are used in our work. Then the slope of the $T(0) \sim I^2$ curve is fitted linearly to determine its slope: $R \cdot L/(4k \cdot A_c)$, from which the thermal conductivity of the sample can be determined directly.

Based on the relationship between temperature and the Raman spectrum, Raman thermometry is a compelling technique for non-contact temperature probing and has been applied successfully on silicon and CNTs analysis [9–11]. Due to the particular structure of CNTs, there are three vibration modes which appear as three peaks in the Raman spectrum: a radial breathing mode (RBM) in the range 100–500 cm^{-1}, a disorder induced D-band at about 1300 cm^{-1} and a graphite-related optical mode (G-band) at around 1600 cm^{-1} [12, 13]. According to the temperature dependence of the Stokes and anti-Stokes effect, there are two approaches that can be used in Raman thermometry. First, the Raman frequency shows a downshift character as the temperature increases [14–17]. Therefore, different temperatures can be distinguished by defining peak positions in specific spectra. However, one disadvantage is the low sensitivity for this method [16]. For example, the temperature coefficient of the G-band frequency is -1.67×10^{-5} K^{-1}. For the RBM mode, this coefficient ranges from -1.06×10^{-5} to -2.3×10^{-4} K^{-1} [14]. Moreover, it is difficult to identify the peak position precisely if the peak is not very sharp (e.g. for MWCNTs). The other approach of temperature sensing is based on the character of the temperature dependence of the peak intensity. It is found that the intensity of the peaks at the D-band and the G-band will decrease as the temperature goes up [15, 18]. The sensitivity of this intensity-based approach is much higher than that of the frequency-based method and will be used in this work.

3 Results and Discussion

CNTs fabricated using different methods may have different Raman spectrum characteristics due to their particular structures in the bundle. In addition, the spectrum may also differ if different probing sources (laser wavelength) are used [19]. The MWCNT bundles used in our experiment are fabricated at the Oak Ridge National Laboratory. The sample bundle is like a cylinder with 4 mm in length and 0.24 mm in diameter. BTC162 High Resolution TE Cooled CCD Array Spectrometer from BWTek Inc is employed in our work to detect the Raman signal. A polarized probing laser installed in front of the spectrometer has a wavelength of 784.22 nm wavelength and 62 mW energy output. Before we conduct the SERT experiment for thermal conductivity characterization, calibration is carried out to establish the relationship between temperature and peak intensity. In this calibration, the MWCNT bundle is attached to a heater with controlled heating power. The temperature of the heater is monitored by a T type thermocouple with 0.13 mm diameter. The thermocouple and the sample are close enough to each other to be considered at the same temperature. When the temperature reaches the steady state, several Raman spectra are obtained with 240 seconds integration time, as shown as Fig. 1(a). The peak of the D-band is preferred for analyzing because it is sharper and has higher intensity than the G-band. The normalized peak intensity versus temperature is shown as Fig. 1(b). It is noted that the normalized intensity reduces to nearly 50% of the initial value when the temperature increases from room temperature to about 160°C. The correlation between them is linearly fitted well with a slope of -3.4×10^{-3} K^{-1}.

In the past, Chiashi et al. established an exponential relationship between temperature and the intensity of the G-band for single-wall CNT (SWCNT) [20]. It shows that the normalized intensity decreased from 0.55 at room temperature to 0.2 at 800 K. The relative sensitivity is -7×10^{-4} K^{-1}, which is much lower than our data. There could be two reasons for this difference. First, the structure difference between MWCNT and SWCNT determines the different temperature dependences. Second, there are different temperature dependence characters between the G-band and D-band due to their formation modes. For the SWCNT sample, the intensity of the G-band is often higher than that of the D-band while the intensity of the D-band is higher than that of the G-band for the MWCNT studied in this work.

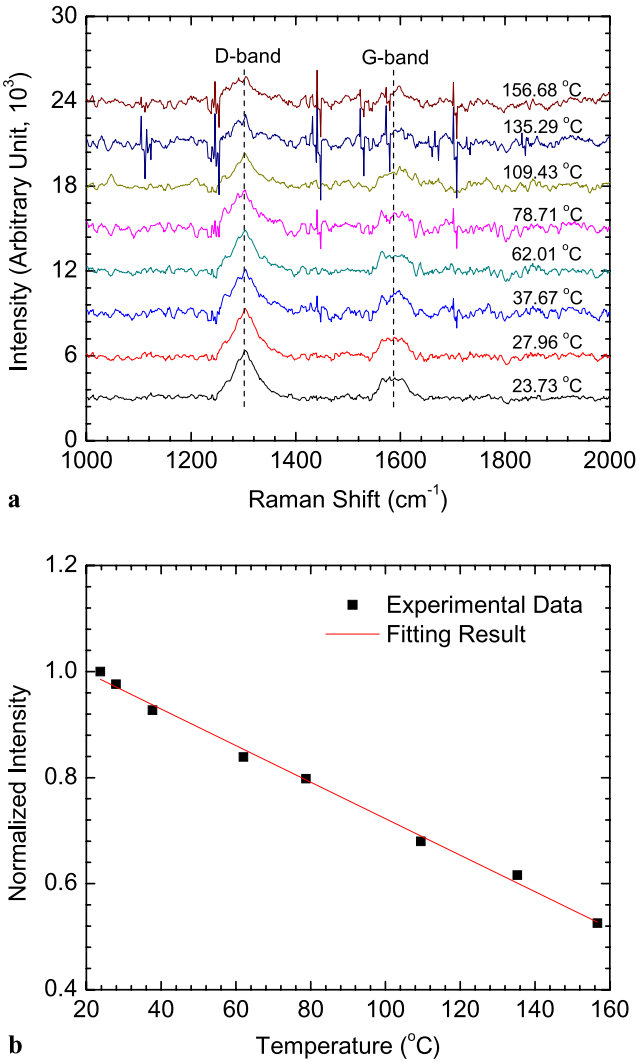

Fig. 1 (**a**) Spectra at different temperatures in calibration experiment, (**b**) the relationship between normalized peak height of D-band and temperature

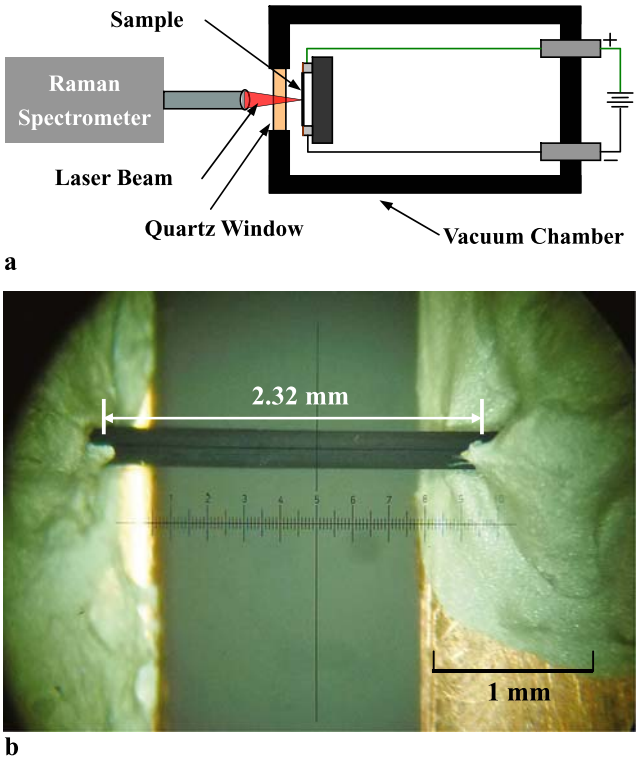

Fig. 2 (**a**) Schematic of the experimental setup for the SERT technique, (**b**) Picture of Sample 1 measured in the experiment

As a result, the temperature dependence of the Raman spectrum should be characterized and treated differently when analyzing different kinds of CNT samples.

The thermal conductivity measurement experiment is carried out in a vacuum chamber with pressure below 1×10^{-3} torr. As shown in Fig. 2(a), the MWCNT sample is suspended between two coplanar copper sheets attached by silver paste. The effective length and diameter of the sample (Sample 1) are 2.32 mm and 0.24 mm respectively and its electrical resistance is 7.0 ohm. The photo of Sample 1 is shown as Fig. 2(b). The copper sheets are connected to the DC power supply for steady-state electrical heating. The electrical current is controlled to increase with larger steps at low values and smaller steps at high values up to 170 mA.

Due to the low pressure in the chamber, the density of air has reduced to a quite low level and the mean free path of air molecules has increased to a few centimeters long. Thus the Fourier law of heat conduction would not be well applicable for this case [1]. The heat conduction from the sample to the adjacent air can be neglected. As a result, only heat conduction along the axial direction of the sample is considered during the steady-state electrical heating. In addition, because of their large volume compared to MWCNTs, the copper sheets and connecting wires have an excellent heat dissipation capacity; the ends of the sample can be assumed to be at the initial room temperature. Therefore, the physical model described above is applicable to calculate the thermal conductivity of MWCNTs.

In the experiment, several spectra are collected at different electrical current values from 0 to 170 mA and the peak intensity at the D-band is normalized. Based on the normalized intensity-temperature relationship obtained in the calibration, the corresponding temperature of different spectra is determined. The correlation between temperature and I^2 is obtained and shown in Fig. 3. Their relationship is linearly fitted with a slope of 3.75×10^3 K/A^2. Considering the middle point temperature of $T(0) = R \cdot L \cdot I^2/(\pi \cdot k \cdot D^2) + T_s$ and applying the fitted value of the slope $R \cdot L/(\pi \cdot k \cdot D^2)$, the thermal conductivity (k) of Sample 1 is calculated as 12.3 W/m·K.

The uncertainty of this experiment mainly comes from two sources: the focus point location of the laser beam and the resistance change during the heating process. If the laser

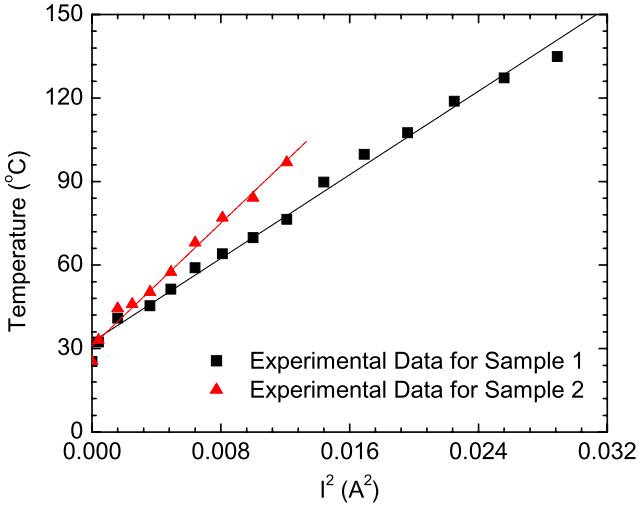

Fig. 3 The correlation between temperature and square of the heating current. The solid lines are the linear fittings of the experimental data

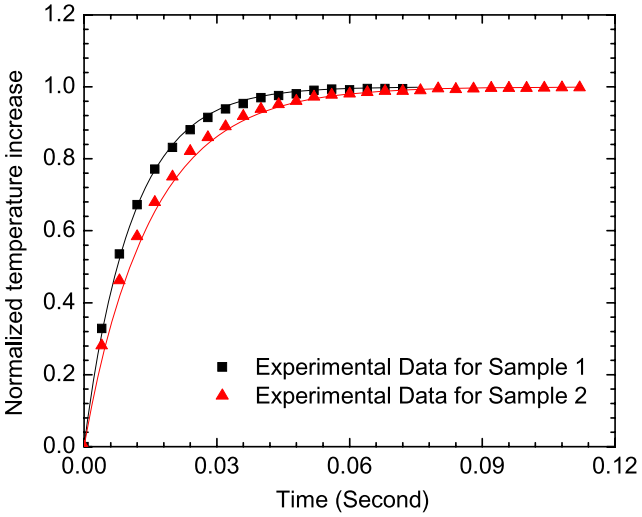

Fig. 4 The normalized temperature increase against time in the TET experiment for two samples

is not focused on the middle point of the sample, for example, assuming that the location shift is 10% of the total length, the x in $T(x) = I^2 \cdot R \cdot L/(4L \cdot k \cdot A_c) \cdot (1 - x^2/L^2) + T_0$ would be $0.2L$. This, in fact, is a very large uncertainty in the laser beam location, and our experiment is carefully controlled to have a much smaller location uncertainty. This large location uncertainty will give only 4% uncertainty in the middle point temperature measurement. In our experiment, it is found that the resistance of Sample 1 changed from 7.0 to 6.8 Ω when the current is increased from 0 to 170 mA. The relative change is about 2.8%, which has negligible effect on the slope value. Another concern is the heating effect of the probing laser of the Raman spectrometer, which will induce some temperature rise in the sample. This heating effect exists for all the electrical currents and will give rise to a shift of the curve, but not the slope. As a result, application of this technique on the thermal conductivity characterization of MWCNT bundles is feasible and physically plausible. To verify the stability of this technique, another MWCNT bundle (Sample 2) with 2.87 mm length and 0.24 mm diameter is measured, again under the same condition. The thermal conductivity is determined as 9.82 W/m·K. The difference between the thermal conductivity of these two bundles can be induced by the structure difference of the bundles, mainly the density of CNTs in the bundle since the bundle is not of full density.

In the above experiment, the SERT technique is used to directly measure the thermal conductivity of MWCNT bundles. If the thermal diffusivity of the sample is available, the density can be determined as well and can be used to validate the above projection. For the thermal diffusivity measurement, the TET technique developed in our group is employed [5]. In this technique, the sample is also suspended between two electrodes and glued with silver paste. Then a

Table 1 Details of experimental results for the two MWCNT samples

	Sample 1	Sample 2
Length (mm)	2.32	2.87
Diameter (mm)	0.24	0.24
Resistance (ohm)	7.00	6.70
Thermal conductivity (W/m·K)	12.3	9.82
Thermal diffusivity (m^2/s)	4.95×10^{-5}	5.00×10^{-5}
Density (kg/m^3)	349	277

periodical electrical heating is induced by applying a square wave AC current on the sample. The heating will cause an evolution of the sample temperature which is tightly related to the heat transfer along the sample. Because the evolution of the sample temperature will cause a variation of its electrical resistance, such a temperature change can be sensed by measuring the variation of the voltage over the sample. Consequently, the thermal diffusivity of the sample can be obtained by fitting the normalized temperature evolution curve against time. The measured temperature evolution of Sample 1 and 2 and the global fitting results are shown in Fig. 4. The thermal diffusivity (α) of Sample 1 and 2 is measured as 4.95×10^{-5} m^2/s and 5.00×10^{-5} m^2/s, respectively. Applying the specific heat of graphite fiber 709 J/kg·K [21], the density is calculated as 349 kg/m^3 and 277 kg/m^3 for Sample 1 and 2, respectively. This shows that Sample 1 has a higher density than Sample 2, explaining its higher thermal conductivity as measured by the SERT technique. The experimental results discussed in this work are summarized in Table 1. Considering differences in structure between the samples, these results are still in good agreement.

In the SERT technology, the Raman spectrum is used to measure the temperature of the sample. Another natural ex-

tension would be to measure the sample's temperature based on its temperature dependence of the electrical resistance. This idea has been tested in our laboratory under steady-state joule heating. It was found that the electrical contact resistance between the sample and electrodes could give an undesired effect on the calibration. This is because, in calibration, the whole sample including the contact points are heated up to the same temperature, while in a real thermal conductivity measurement, the contact points are usually at room temperature, while the sample is heating up. Such an effect is more important for low electrical resistance samples. For the development and measurement reported in this work, the middle point temperature increase of the sample is measured using Raman thermometry. For very short samples, for example, samples with a length much shorter than the focal point size of the probing laser of the Raman spectrometer, the average temperature $[=I^2 \cdot R \cdot L/(6k \cdot A_c) + T_0]$ of the sample can be measured instead of its middle point temperature. In this way, the SERT technique can be applied to measure the thermal conductivity of very short samples.

4 Conclusion

In summary, a novel steady-state electro-Raman-thermal technique—SERT—was developed to directly measure the thermal conductivity of MWCNT bundles. The reported SERT technique provides an advanced way to characterize the thermal conductivity of one-dimensional micro/nanoscale structures by either measuring its middle point temperature or average temperature increase (for very short nanowires) under steady-state electrical heating. In addition, combined with the TET method to measure the sample's thermal diffusivity, its density was also obtained precisely. The thermal conductivity, thermal diffusivity and density of two measured MWCNT bundles were 12.3 and 9.82 W/m·K, 5.00×10^{-5} and 4.95×10^{-5} m^2/s, and 349 and 277 kg/m^3, respectively.

Acknowledgements Support of this work from the start-up fund of Iowa State University is gratefully acknowledged. X. Wang also very much appreciates the discussion with Professor Yongfeng Lu of the University of Nebraska-Lincoln during the development of the SERT technique.

References

1. J. Hou, X. Wang, P. Vellelacheruvu, J. Guo, C. Liu, H.-M. Cheng, J. Appl. Phys. **100**, 124314 (2006)
2. P. Kim, L. Shi, A. Majumdar, P.L. Mceuen, Phys. Rev. Lett. **87**, 215502 (2001)
3. L. Shi, Q. Hao, C. Yu, N. Mingo, X. Kong, Z.L. Wang, Appl. Phys. Lett. **84**, 2638–2640 (2004)
4. J. Hou, X. Wang, L. Zhang, Appl. Phys. Lett. **89**, 152504 (2006)
5. J. Guo, X. Wang, T. Wang, J. Appl. Phys. **101**, 063537 (2007)
6. J. Guo, X. Wang, L. Zhang, T. Wang, Appl. Phys. A **89**, 153–156 (2007)
7. T. Wang, X. Wang, J. Guo, Z. Luo, K. Ceng, Appl. Phys. A **87**, 599–605 (2007)
8. J. Guo, X. Wang, D.B. Geohegan, G. Eres, C. Vincent, J. Appl. Phys. **103**, 113505 (2008)
9. R. Tsu, J.G. Hernandez, Appl. Phys. Lett. **41**, 1015–1018 (1982)
10. I.K. Hsu, R. Kumar, A. Bushmaker, S.B. Cronin, M.T. Pettes, L. Shi, T. Brintlinger, M.S. Fuhrer, J. Cumings, Appl. Phys. Lett. **92**, 063119 (2008)
11. F. Huang, K.T. Yue, P. Tan, S.-L. Zhang, Z. Shi, X. Zhou, Z. Gu, J. Appl. Phys. **84**, 4022–4024 (1998)
12. E.F. Antunes, A.O. Lobo, E.J. Corat, V.J. Trava-Airoldi, A.A. Martin, C. Veríssimo, Carbon **44**, 2202–2211 (2006)
13. S. Costa, E. Borowiak-Palen, M. Kruszyñska, A. Bachmatiuk, R.J. Kalenczuk, Mater. Sci. **26**, 433–441 (2008)
14. Y. Zhang, L. Xie, J. Zhang, Z. Wu, Z. Liu, J. Phys. Chem. C **111**, 14031–14034 (2007)
15. L. Song, W. Ma, Y. Ren, W. Zhou, S. Xie, P. Tan, L. Sun, Appl. Phys. Lett. **92**, 121905 (2008)
16. Z. Zhou, X. Dou, L. Ci, L. Song, D. Liu, Y. Gao, J. Wang, L. Liu, W. Zhou, S. Xie, D. Wan, J. Phys. Chem. B **110**, 1206–1209 (2006)
17. Q. Zhang, D.J. Yang, S.G. Wang, S.F. Yoon, J. Ahn, Smart Mater. Struct. **15**, S1–S4 (2006)
18. Z.H. Ni, H.M. Fan, X.F. Fan, H.M. Wang, Z. Zheng, Y.P. Feng, Y.H. Wu, Z.X. Shen, J. Raman Spectrosc. **38**, 1449–1453 (2007)
19. K. Behler, S. Osswald, H. Ye, S. Dimovski, Y. Gogotsi, J. Nanopart. Res. **8**, 615–625 (2006)
20. S. Chiashi, Y. Murakami, Y. Miyauchi, S. Maruyama, Therm. Sci. Eng. 71–72 (2005)
21. F.P. Incropera, D.P. Dewitt, T.L. Bergman, A.S. Lavine, *Fundamentals of Heat and Mass Transfer*, 6th edn. (Wiley, New York, 2007)